Acta Mech 199, 17–28 (2008)
DOI 10.1007/s00707-007-0563-4
Printed in The Netherlands

Acta Mechanica

The impulse response of a band-limited vibrator with rate-independent hysteretic damping

K. F. Chen[1], Y. H. Shen[2]

[1] College of Science, China Agricultural University, Beijing, P.R. China
[2] School of Civil and Environmental Engineering, University of Science and Technology, Beijing, P.R. China

Received 28 October 2007; Accepted 26 November 2007; Published online 14 February 2008

Summary. The linear rate-independent damping model is non-causal. But its mathematical form is so attractive that this model and its enhancements are still considered as contemporary research. The linear band-limited hysteretic vibrator (LBLHV) is one such suggested modification for suppressing the non-causality effect. However, its response properties have not been delineated. One of the properties, the unitary impulse response function, will be investigated systematically by the residue theorem here. It was shown that, first, the LBLHV is still non-causal, and the asymptotic rate of the impulse response precursor (IRP) is $O(1/t)$ as time approaches negative infinity. Second, the IRP is no longer monotonic, but composed of two oscillating components. Third, the response at $t = 0$ can be set to zero by appropriately combining the lower and upper limits of the pass band.

1 Introduction

Consideration of damping is fundamental to vibration and wave analysis [1], [2]. Thus, a simple but accurate damping model is needed. A linear viscous damping model is the simplest from a theoretical point of view. This model stipulates that the energy loss per cycle of vibration is proportional to the vibration frequency [3]. A more general damping model assumes that the energy loss per cycle varies with the vibration frequency [4]–[7]. Extensive experiments showed that the simplest form – a frequency independent model – could follow the damping properties of many materials, e.g., those of soil [8] and two contacting surfaces of elastic solids [9]. This frequency-independent or rate-independent damping model has other names such as the linear hysteretic damping, structural damping, material damping, complex stiffness [10], [11], and internal damping.

The rate independent model is linear. The unitary impulse response function (UIRF) is another description of a linear system. The UIRF is the response after the system is excited by a unitary input at $t = 0$. For a physical realizable system, no response occurs before $t = 0$, that is the UIRF is zero for $t < 0$. The system possessing this property is called the causal system. The hysteretic model is

Correspondence: Kui Fu Chen, College of Science, China Agricultural University, P.B. 74, East Campus, Beijing 100083, P.R. China
e-mail: chenkuifu@gmail.com

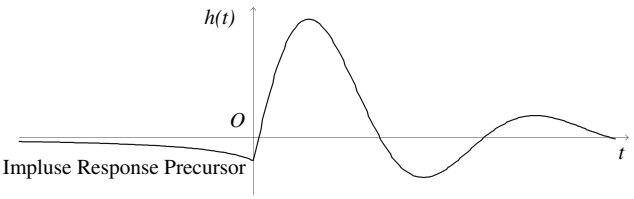

Fig. 1. The unitary impulse response function of the hysteretic model and the impulse response precursor (*IRP*)

the mathematical revision from the viscous damping model, which is causal. The UIRF of a hysteretically damped vibrator is shown in Fig. 1, where the UIRF is not zero for $t < 0$. This non-causality phenomenon has been proved rigorously [10]–[18]. In some literature, the nonzero UIRF for $t < 0$ is termed the impulse response precursor (IRP).

The IRP is somewhat inconsistent from the physical viewpoint. One strategy to avoid the non-causality is to replace the rate-independent damping model with a revised one. Makris [19] had instrumented such kind of model. However, the new model stiffness is no longer a constant anyhow. Muravskii [20] has constructed a model with nearly frequency independent complex stiffness which can lead to causal behavior. Maia et al. [21] attempted to eliminate the non-causality by introducing both *the complex response in the time domain* and complex initial conditions. However, the physical meaning of the imaginary part of the response needs further clarification. Nakamura [22] presented a practical hysteretic damping model which satisfies the causality condition recently.

Another strategy is just to ignore the IRP, which is achieved either implicitly or explicitly. For example, if the impulse response function is used explicitly, the IRP is simply regarded as zero. For an implicit way, for example, in frequency domain analysis, the contribution from non-causality is minor for a lightly damped system, and can be neglected from a practical point of view [23]. Sometimes, the hysteretic damping is replaced with viscous damping to facilitate analysis [24]–[26]. Approximating the hysteretic damping matrix with a viscous matrix was studied systematically by Henwood et al. [27]. But, it has also been shown that in some cases the inaccuracy associated with the use of an equivalent viscous damping model is rather significant [28].

The band-limited hysteretic damper, proposed by Bishop and Price [29], is also one of such remedies, made to suppress the non-causal behavior. Crandall [30] has verified that this band-limited damper itself is non-causal. However, a vibrating system usually has a mass and a spring in addition to the damper.

It still needs to be clarified whether a band-limited system with rate-independent damping is causal or not. If the model is non-causal, can we manipulate some conditions to make the non-causal degree as small as possible? This arises another question, how can we quantify the non-causal size? For the ideal case, the IRP maximizes at $t = 0$. This paper answers the following question: does this property still hold for the band-limited case? If this does not, then can we find the maximum of IRP? Moreover, is the IRP still monotonic?

In this paper the UIRF will be derived through the residue theorem. The important properties of UIRF will be investigated at great length.

2 The mathematical model

The governing equation of a single-degree-of-freedom vibrator with a viscous damper is

$$m\ddot{x} + c\dot{x} + kx = f(t). \tag{1}$$

Here m, c and k are the system's mass, viscous damping coefficient, and stiffness, respectively, $f(t)$ is the excitation and $x(t)$ the response. Its frequency response function is

$$H(j\omega) = \frac{1}{-m\omega^2 + jc\omega + k}. \tag{2}$$

The Coulomb friction force is a good model under a low velocity condition, and its mathematical expression is $\tilde{c}\dot{x}/|\dot{x}|$, where $\tilde{c}$ is the coefficient of friction. If this model takes over the viscous model in Eq. (1), the following nonlinear model results:

$m\ddot{x} + \tilde{c}\dot{x}/|\dot{x}| + kx = f(t)$.

It can be proved that the damping contribution in this model is independent of the excitation frequency if the system is excited by a harmonic input. As mentioned before and experimentally verified, this frequency independent damping model is valid for many kinds of material. But the nonlinear model is not easy to analyze, therefore some researchers replaced the contribution term of viscous damping $jc\omega$ with $j\tilde{c}\,\mathrm{sign}(\omega)$, leading to the following transfer function:

$$H(j\omega) = \frac{1}{m(j\omega)^2 + \tilde{c}j\,\mathrm{sign}\omega + k}. \tag{3}$$

Crandall [30], [31] called this the ideal hysteretic model. Just as shown in Fig. 1, this model is non-causal, and several modifications have been proposed as cited in the Introduction Section. The linear band-limited hysteretic vibrator (LBLHV) is one such revision, and the corresponding transfer function follows as

$$H(j\omega) = \begin{cases} \dfrac{1}{m(j\omega)^2 + k(1 + j\eta\,\mathrm{sign}\omega)} & \Omega_\mathrm{L} < |\omega| < \Omega_\mathrm{H} \\ 0 & |\omega| < \Omega_\mathrm{L} \text{ or } |\omega| > \Omega_\mathrm{H} \end{cases}. \tag{4}$$

$\eta > 0$ is the dimensionless loss-factor. Ω_H and Ω_L are the upper bound and lower bound of the pass frequency band, respectively. We further assume that

$$\Omega_\mathrm{L} < \mu\omega_n \quad \text{and} \quad \Omega_\mathrm{H} \geqslant \omega_n(\mu^2 + \lambda^2) = \omega_n\sqrt{1 + \eta^2}. \tag{5}$$

Here, $\omega_n = \sqrt{k/m}$ is the circular natural frequency without damping. And λ and μ are

$$\lambda = \sqrt{(\sqrt{1 + \eta^2} - 1)/2} \quad \text{and} \quad \mu = \sqrt{(\sqrt{1 + \eta^2} + 1)/2}.$$

The LBLHV of Eq. (4) deteriorates to the ideal hysteretic case if Ω_H is infinite and Ω_L is zero [19].

The UIRF $h(t)$ relates with the frequency response function $H(j\omega)$ via the inverse Fourier transform as follows:

$$h(t) = \frac{1}{2\pi}\int_{-\infty}^{+\infty} H(j\omega)\exp(j\omega t)d\omega. \tag{6}$$

In the ensuing study, we use the contour integration and residue theorem to evaluate the above equation. First, the frequency response function needs to be extended to the transfer function. This is obtained by substituting $j\omega$ in Eq. (4) with the complex $s = j\omega + \sigma$. On the complex plane depicted in Fig. 2, the transfer function is

$$H(s) = \begin{cases} \dfrac{1}{ms^2 + k\{1 + j\eta\,\mathrm{sign}[\mathrm{Im}(s)]\}} & \Omega_\mathrm{L} < |\mathrm{Im}(s)| < \Omega_\mathrm{H} \\ 0 & |\mathrm{Im}(s)| < \Omega_\mathrm{L} \text{ or } |\mathrm{Im}(s)| > \Omega_\mathrm{H} \end{cases}.$$

Its two poles are as follows:

$z_1 = (j\mu - \lambda)\omega_n, \quad z_2 = (-j\mu - \lambda)\omega_n.$

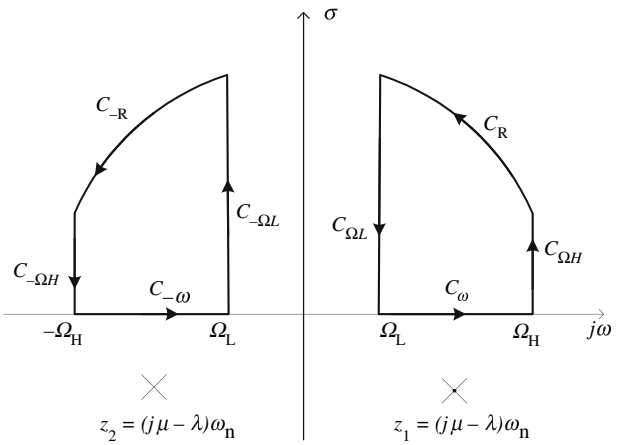

Fig. 2. Integral contours for the IRP

3 The impulse response precursor

3.1 Theoretical analysis

The IRP is defined over the negative time. According to the band-limited assumption for $H(j\omega)$ and Eq. (6), we have

$$h(t) = \frac{1}{2\pi}\int_{\Omega_H}^{\Omega_L} H(j\omega)\exp(j\omega t)d\omega + \frac{1}{2\pi}\int_{-\Omega_H}^{-\Omega_L} H(j\omega)\exp(j\omega t)d\omega. \tag{7}$$

The integration contours for the residual theorem are chosen on the upper half of the complex plane (For $t > 0$, such a choice can make use of the asymptotical property of the integrands of Eq. (7) as $t \to \infty$). This is depicted in Fig. 2, $C_\omega \to C_{\Omega_H} \to C_R \to C_{\Omega_L}$ and $C_{-\omega} \to C_{-\Omega_L} \to C_{-R} \to C_{-\Omega_H}$. Inside these loops, $H(s)$ is analytical. Equation (7) correlates with the integral along C_ω and $C_{-\omega}$ as follows:

$$h(t) = \frac{1}{j2\pi}\left[\int_{C_\omega} H(s)\exp(st)ds + \int_{C_{-\omega}} H(s)\exp(st)ds\right]. \tag{8}$$

Now we consider $C_\omega \to C_{\Omega_H} \to C_R \to C_{\Omega_L}$. Since this loop lies within the analytical domain and does not encircle any pole, the following equation holds true in the light of the residue theorem:

$$\begin{aligned}\int_{C_\omega} H(s)\exp(st)ds + \int_{C_{\Omega_H}} H(s)\exp(st)ds + \int_{C_R} H(s)\exp(st)ds \\ + \int_{C_{\Omega_L}} H(s)\exp(st)ds = 0.\end{aligned} \tag{9}$$

On the upper half of the complex plane, the third term will vanish as the radius R of the arc C_R approaches infinity. This is because the integrand $|H(s)\exp(st)| \le |H(s)| = O(R^{-2})$ as $R \to \infty$. Thus

$$\int_{C_\omega} H(s)\exp(st)ds = -\int_{C_{\Omega_H}} H(s)\exp(st)ds - \int_{C_{\Omega_L}} H(s)\exp(st)ds. \tag{10}$$

As $R \to \infty$, the second term of Eq. (9) becomes

$$\int_{C_{\Omega_{\mathrm{H}}}} H(s)\exp(st)ds = \exp(j\Omega_{\mathrm{H}}t)\int_{0}^{\infty} H(\sigma + j\Omega_{\mathrm{H}})\exp(\sigma t)d\sigma. \tag{11}$$

It can be written in a compact form,

$$\int_{C_{\Omega_{\mathrm{H}}}} H(s)\exp(st)ds = \exp(j\Omega_{\mathrm{H}}t)\Psi(\Omega_{\mathrm{H}}, t), \tag{12}$$

where $\Psi(\Omega, t)$ is an auxiliary function defined as follows:

$$\Psi(\Omega, t) = \int_{0}^{\infty} H(\sigma + j\Omega)\exp(\sigma t)d\sigma. \tag{13}$$

As $R \to \infty$, the fourth term of Eq. (9) becomes

$$\int_{C_{\Omega_{\mathrm{L}}}} H(s)\exp(st)ds = \exp(j\Omega_{\mathrm{L}}t)\int_{\infty}^{0} H(\sigma + j\Omega_{\mathrm{L}})\exp(\sigma t)d\sigma. \tag{14}$$

Inverting the integral limits of the right-hand side leads to

$$\int_{C_{\Omega_{\mathrm{L}}}} H(s)\exp(st)ds = -\exp(j\Omega_{\mathrm{L}}t)\int_{0}^{\infty} H(\sigma + j\Omega_{\mathrm{L}})\exp(\sigma t)d\sigma. \tag{15}$$

Thus,

$$\int_{C_{\Omega_{\mathrm{L}}}} H(s)\exp(st)ds = -\exp(j\Omega_{\mathrm{L}}t)\Psi(\Omega_{\mathrm{L}}, t). \tag{16}$$

Substitution of Eqs. (12) and (16) into Eq. (10) yields

$$\int_{C_{\omega}} H(s)\exp(st)ds = \exp(j\Omega_{\mathrm{L}}t)\Psi(\Omega_{\mathrm{L}}, t) - \exp(j\Omega_{\mathrm{H}}t)\Psi(\Omega_{\mathrm{H}}, t). \tag{17}$$

For the loop of $C_{-\omega} \to C_{-\Omega_{\mathrm{L}}} \to C_{-R} \to C_{-\Omega_{\mathrm{H}}}$, in the same vein, we have

$$\int_{C_{-\omega}} H(s)\exp(st)ds = \exp(-j\Omega_{\mathrm{H}}t)\Psi(-\Omega_{\mathrm{H}}, t) - \exp(-j\Omega_{\mathrm{L}}t)\Psi(-\Omega_{\mathrm{L}}, t). \tag{18}$$

Substitution of Eqs. (16) and (18) into Eq. (8) leads to

$$\begin{aligned} h(t) = \frac{1}{2\pi}\mathrm{Im}[&\exp(-j\Omega_{\mathrm{H}}t)\Psi(-\Omega_{\mathrm{H}}, t) - \exp(-j\Omega_{\mathrm{L}}t)\Psi(-\Omega_{\mathrm{L}}, t) \\ &+ \exp(j\Omega_{\mathrm{L}}t)\Psi(\Omega_{\mathrm{L}}, t) - \exp(j\Omega_{\mathrm{H}}t)\Psi(\Omega_{\mathrm{H}}, t)]. \end{aligned} \tag{19}$$

In light of the conjugate property of $H(j\omega)$ of Eq. (4) and the definition of $\Psi(\Omega, t)$ by Eq. (12), we have the property of conjugate symmetry $\Psi^*(\Omega, t) = \Psi(-\Omega, t)$. Thus, Eq. (19) can be further simplified to

$$h(t) = \mathrm{Im}[\exp(j\Omega_{\mathrm{L}}t)\Psi(\Omega_{\mathrm{L}}, t) - \exp(j\Omega_{\mathrm{H}}t)\Psi(\Omega_{\mathrm{H}}, t)]/\pi. \tag{20}$$

3.2 Numerical computation

The explicit expression of $h(t)$ is not feasible, so a numerical approach is necessary. To achieve this, we turn to $\Psi(\Omega, t)$, which is

$$\begin{aligned}\Psi(\Omega,t) &= \int_0^\infty \frac{\exp(\sigma t)}{m\left[\omega_n^2 + (\sigma + j\Omega)^2 + j\eta\omega_n^2\right]}d\sigma \\ &= \frac{1}{m\omega_n}\int_0^\infty \frac{\exp(\sigma\omega_n t)}{1 + j\eta + (\sigma + j\alpha)^2}d\sigma,\end{aligned} \tag{21}$$

where $\alpha = \Omega/\omega_n > 0$ is the normalized frequency.

For the purpose of facilitating numerical computation, the entire infinite integrating range $[0, +\infty)$ is dissected into two bands, $[0, v)$ and $[v, +\infty)$. For a sufficiently large v, the following approximation holds:

$$\frac{1}{1 + j\eta + (\sigma + j\alpha)^2} \approx \frac{1}{\sigma^2} \quad \text{for } \sigma > v. \tag{22}$$

Thus,

$$\Psi(t) \approx \frac{1}{m\omega_n}\left[\int_0^v H_0(\sigma)\exp(\sigma\omega_n t)d\sigma + \frac{1}{v}E_2(-v\omega_n t)\right]. \tag{23}$$

The first term in the square bracket of Eq. (23) can be obtained by a conventional numerical integration. $E_k(x)$ in Eq. (23) is the exponential integral as follows:

$$E_k(x) = \int_1^\infty \frac{\exp(-x\sigma)}{\sigma^k}d\sigma. \tag{24}$$

Computation of the exponential integral is discussed in detail in [32]. The efficient algorithm depends on the argument size x. For a large $x > 1$, the continued fraction is used, while for a small x ($\leq$1) the series representation is preferred.

3.3 Remarks

The IRP of a typical band-limited hysteretic vibrator is shown in Fig. 3, along with the IRP of the ideal case. For the system parameters and computational parameters, see the Figure's illustration. Examining this Figure leads to the following conclusions.

First, the IRP approaches zero as time approaches negative infinity. This can be argued as follows. In light of Eq. (20)

$$|h(t)| \leqslant [|\Psi(\Omega_{\mathrm{L}}, t)| + |\Psi(\Omega_{\mathrm{H}}, t)|]/\pi. \tag{25}$$

According to Eq. (21), we have

$$|\Psi(\Omega,t)| \leqslant \frac{1}{m\omega_n}\int_0^\infty \frac{\exp(\sigma\omega_n t)}{|1 + j\eta + (\sigma + j\alpha)^2|}d\sigma = \frac{1}{m\omega_n}\int_0^\infty \frac{\exp(\sigma\omega_n t)}{\sqrt{\zeta(\sigma,\eta,\alpha)}}d\sigma, \tag{26}$$

where the term under the square root symbol is

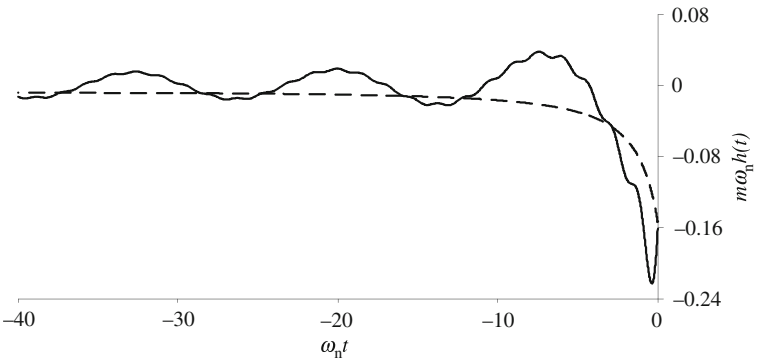

Fig. 3. The IRPs *solid* and *dashed lines* stand for the band-limited case and the ideal case, respectively. The loss-factor $\eta = 0.9$ for both cases. The Ω_H and Ω_{L} for the band-limited case are equal to $0.4\omega_n$ and $4\omega_n$, respectively. The computational parameters are $v = 100\omega_n$, and $\Delta\omega = 0.1\omega_n$ for the trapezoidal numerical integration for the first term of Eq. (24)

$$\begin{aligned}\zeta(\sigma,\eta,\alpha) &= (1+\sigma^2-\alpha^2)^2 + (\eta+2\sigma\alpha)^2 \\ &= \sigma^4 + 2\sigma^2 + 2\sigma^2\alpha^2 + 4\eta\sigma\alpha + 1 - 2\alpha^2 + \alpha^4 + \eta^2.\end{aligned} \tag{27}$$

Evidently, for $\sigma > 0$

$$\zeta(\sigma,\eta,\alpha) \geqslant (1-\alpha^2)^2 + \eta^2. \tag{28}$$

Thus,

$$|\Psi(\Omega,t)| \leqslant \frac{1}{m\omega_n}\int_0^\infty \frac{\exp(\sigma\omega_n t)}{\sqrt{(1-\alpha^2)^2+\eta^2}}d\sigma = \frac{1}{m\omega_n^2\sqrt{(1-\alpha^2)^2+\eta^2}}\frac{1}{-t}. \tag{29}$$

According to Eq. (25), we have

$$|h(t)| \leqslant = \frac{1}{m\omega_n^2}\left[\frac{1}{\sqrt{(1-\alpha_{\mathrm{L}}^2)^2+\eta^2}} + \frac{1}{\sqrt{(1-\alpha_{\mathrm{H}}^2)^2+\eta^2}}\right]\frac{1}{-t}. \tag{30}$$

Obviously, the summation in the square bracket is finite. Thus we have proved that IRP approaches zero as time approaches negative infinity. Anyhow, like in the ideal hysteretic case, the attenuating rate is very low, only of the order $O(|t|^{-1})$.

Second, unlike the ideal case, the IRP trend is not monotonic. Basically, the fluctuation consists of two components, the slow $h_{\mathrm{L}}(t)$ and the fast $h_{\mathrm{H}}(t)$. That is,

$$h(t) = h_{\mathrm{L}}(t) + h_{\mathrm{H}}(t), \tag{31}$$

where

$$\begin{aligned}h_{\mathrm{L}}(t) &= \mathrm{Im}[\exp(j\Omega_{\mathrm{L}}t)\Psi(\Omega_{\mathrm{L}},t)]/\pi \\ h_{\mathrm{H}}(t) &= -\mathrm{Im}[\exp(j\Omega_{\mathrm{H}}t)\Psi(\Omega_{\mathrm{H}},t)]/\pi.\end{aligned} \tag{32}$$

The slow component originates from the lower boundary Ω_{L}. As $\Omega_{\mathrm{L}} \to 0, h_{\mathrm{L}}(t) \to \mathrm{Im}[\Psi(0,t)]/\pi$. $\mathrm{Im}[\Psi(0,t)]/\pi$ is nothing but the IRP of the ideal hysteretic case. We have shown that $\mathrm{Im}[\Psi(0,t)]/\pi$ is monotonic over the negative time [33].

Third, the fast component correlates to the high boundary Ω_{H}. Numerical simulation shows that this component diminishes as $\Omega_{\mathrm{H}} \to \infty$. This can be argued stringently. In light of Eq. (29),

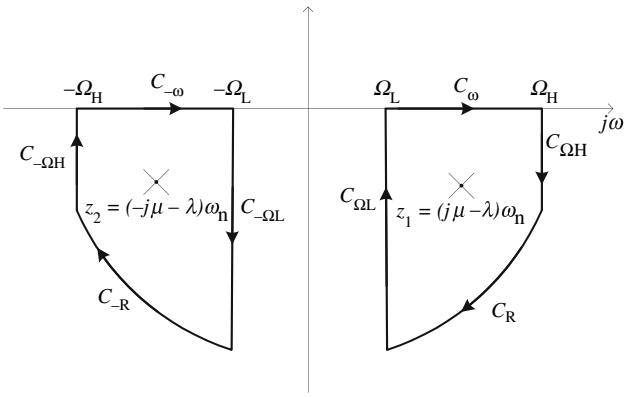

Fig. 4. Integral contours for $t > 0$

$|\Psi(\Omega, t)| \to 0$ as $\alpha = \Omega_H/\omega_n \to \infty$. The authors think that the fluctuation artifact shown in Fig. 4 by Gaul et al. [13] may be ascribed to the fact that the frequency truncation of numerical computation is too low. In their paper, the IRP was approximated by a numerical approach.

The fourth point is that, unlike the ideal case, $h(t)$ is not maximum at the origin. Thus evaluating the non-causal degree is more difficult than in the ideal case. We should calculate the IRP at least over the period $(-\pi/\Omega_H, 0]$ and use the extremum over this period as the non-causal index.

4 Response for $t > 0$

A realistic vibrator is causal, that is, a response occurs only after an impulse. For the above artificial system, we are definitely interested in the impulse response function for $t > 0$. Now, Eq. (6) still holds, but the integral routes must be placed in the lower half of the complex plane, as shown in Fig. 4.

Now, we consider $C_\omega \to C_{\Omega_H} \to C_R \to C_{\Omega_L}$, inside which $H(s)$ possesses a pole. The following equation holds in the light of the residue theorem (noting that $H(s)$ equals $1/[m(s - z_1)(s + z_1)]$ inside this loop):

$$\int_{C_\omega} H(s)\exp(st)ds + \int_{C_{\Omega_H}} H(s)\exp(st)ds + \int_{C_R} H(s)\exp(st)ds + \int_{C_{\Omega_L}} H(s)\exp(st)ds = 2\pi j Res[H(z)\exp(zt)]|_{s=z_1} = \frac{2\pi j \exp(z_1 t)}{2mz_1}. \tag{33}$$

As $R \to$ infinity (noting the route direction), we have

$$\int_{C_R} H(s)\exp(st)ds = 0. \tag{34}$$

The second term of Eq. (33) is

$$\begin{aligned}\int_{C_{\Omega_H}} H(s)\exp(st)ds &= \int_0^{-\infty} H(\sigma + j\Omega_H)\exp[(\sigma + j\Omega_H)t]d\sigma \\ &= \int_0^{\infty} H(-\sigma + j\Omega_H)\exp[(-\sigma + j\Omega_H)t]d(-\sigma) \\ &= -\exp(j\Omega_H t)\tilde{\Psi}(\Omega_H, t),\end{aligned} \tag{35}$$

where

$$\tilde{\Psi}(\Omega, t) = \int_0^\infty H(-\sigma + j\Omega)\exp(-\sigma t)d\sigma.$$

Similar to $\Psi(\Omega, t)$, this function also possesses the conjugate symmetry as $\tilde{\Psi}(-\Omega_{\mathrm{H}}, t) = \tilde{\Psi}^*(\Omega_{\mathrm{H}}, t)$. Similarly,

$$\int_{C_{\Omega_{\mathrm{L}}}} H(s)\exp(st)ds = \exp(j\Omega_{\mathrm{L}}t)\tilde{\Psi}(\Omega_{\mathrm{L}}, t). \tag{36}$$

Combining Eq. (33)–Eq. (36) together one obtains

$$\int_{C_\omega} H(s)\exp(st)ds = \frac{2\pi j\exp(z_1 t)}{2mz_1} + [-\exp(j\Omega_{\mathrm{L}}t)\tilde{\Psi}(\Omega_{\mathrm{L}}, t) + \exp(j\Omega_{\mathrm{H}}t)\tilde{\Psi}(\Omega_{\mathrm{H}}, t)]. \tag{37}$$

For the loop $C_{-\omega} \to C_{-\Omega_{\mathrm{L}}} \to C_{-R} \to C_{-\Omega_{\mathrm{H}}}$ in Fig. 4, the following equation holds true:

$$\int_{C_{-\omega}} H(s)\exp(st)ds = \frac{2\pi j\exp(z_2 t)}{2mz_2} + [-\exp(-j\Omega_{\mathrm{L}}t)\tilde{\Psi}(-\Omega_{\mathrm{L}}, t) + \exp(-j\Omega_{\mathrm{H}}t)\tilde{\Psi}(-\Omega_{\mathrm{H}}, t)]. \tag{38}$$

Thus,

$$h(t) = \frac{\exp(-\lambda\omega_n t)[\mu\sin(\mu\omega_n t) - \lambda\cos(\mu\omega_n t)]}{m\omega_n(\mu^2 + \lambda^2)} + \frac{\mathrm{Im}[\exp(j\Omega_{\mathrm{H}}t)\tilde{\Psi}(\Omega_{\mathrm{H}}, t) - \exp(j\Omega_{\mathrm{L}}t)\tilde{\Psi}(\Omega_{\mathrm{L}}, t)]}{\pi}. \tag{39}$$

Four typical UIRFs are shown in Fig. 5. We can find the nonzero dips at $t = 0$. Nonetheless, the UIRFs are continuous here. Further, they are smooth at $t = 0$ if Ω_{H} is finite. The UIRFs for $t > 0$ are dominated by a damped oscillation, similar to a viscous model. In light of Eq. (39), they should contain three oscillating components from the lower limit Ω_{L}, the upper limit Ω_{H}, and the natural frequency ω_n. But the third factor prevails over the first two, thus only the component pertaining to the natural frequency appears from a global view. The difference between the ideal case and the band-limited one manifests significantly at the first peak. As time develops, this difference fades.

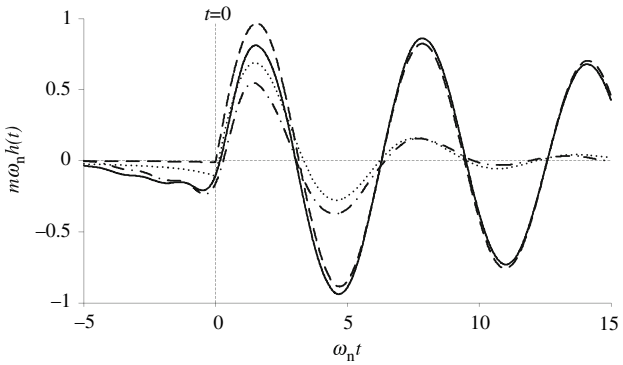

Fig. 5. Unitary impulse response functions of four typical cases. The four cases are *dash-dotted line* for $\eta = 0.5$, $\Omega_{\mathrm{H}} = 4\omega_n$, $\Omega_{\mathrm{L}} = 0.5\omega_n$; *dotted line* for $\eta = 0.5$, $\Omega_{\mathrm{H}} = \infty$, $\Omega_{\mathrm{L}} = 0$; *solid line* for $\eta = 0.05$, $\Omega_{\mathrm{H}} = 4\omega_n$, $\Omega_{\mathrm{L}} = 0.5\omega_n$; and *dashed line* for $\eta = 0.05$, $\Omega_{\mathrm{H}} = \infty$, $\Omega_{\mathrm{L}} = 0$. Other computational parameters confer to Fig. 3

5 Response size at $t = 0$

It has been proved that the IRP becomes maximum at the origin ($t = 0$) for the ideal hysteretic model, thus the response at $t = 0$, $h(0)$, is an apt index to quantify the non-causal size [33]. However, as mentioned above, this property does not hold true for the band-limited model, since the IRP is non-monotonic. But $h(0)$ is still significant since the value at the origin is of special interest.

It is noteworthy that in both instances of η in Fig. 5, $h(0)$ of the band-limited model is even larger than that of the ideal case. Ironically, the initial purpose of introducing the band-limited model was to alleviate the non-causal feature. However, the parameters Ω_{L} and Ω_{H} give us freedom to manipulate the size of $h(0)$. In light of Eq. (20), we have

$$h(0) = \frac{\mathrm{Im}[\Psi(\Omega_{\mathrm{L}}, 0) - \Psi(\Omega_{\mathrm{H}}, 0)]}{\pi}. \tag{40}$$

After a bit of tedious deduction, we can find a closed-form expression of $\mathrm{Im}[\Psi(\Omega, 0)]$ to be

$$\begin{aligned}\mathrm{Im}[\Psi(\Omega, 0)] = {} & \frac{1}{m\omega_n}\frac{\mu}{2(\lambda^2+\mu^2)}\ln\sqrt{\frac{\lambda^2+(\alpha-\mu)^2}{\lambda^2+(\alpha+\mu)^2}} \\ & - \frac{\lambda}{2m\omega_n(\lambda^2+\mu^2)}\left\{\frac{\pi[1-\mathrm{sign}(\alpha-\mu)]}{2} + \arctan\frac{\lambda}{\alpha-\mu} + \arctan\frac{\lambda}{\alpha+\mu}\right\},\end{aligned} \tag{41}$$

where α on the right-hand side stands for $\alpha = \Omega/\omega_n$. The presumptions of $\alpha_{\mathrm{L}} = \Omega_{\mathrm{L}}/\omega_n < \mu$ and $\alpha_{\mathrm{H}} = \Omega_{\mathrm{H}}/\omega_n > \mu^2 + \lambda^2$ [cf. Eq. (5)] lead to

$$h(0) = \frac{1}{m\omega_n}\frac{\lambda}{2(\lambda^2+\mu^2)}[-1 + \Phi(\alpha_{\mathrm{L}}) - \Phi(\alpha_{\mathrm{H}})], \tag{42}$$

where

$$\Phi(\alpha) = \frac{1}{\pi}\left[\frac{\mu}{\lambda}\ln\sqrt{\frac{\lambda^2+(\alpha-\mu)^2}{\lambda^2+(\alpha+\mu)^2}} - \arctan\frac{\lambda}{\alpha-\mu} - \arctan\frac{\lambda}{\alpha+\mu}\right]. \tag{43}$$

It is easy to verify that $\Phi(\alpha) \to 0$ for both $\alpha \to 0$ and $\alpha \to \infty$. Hence, as $\alpha \to 0$ and $\alpha \to \infty$, $h(0)$ approaches the value of the ideal case, $-\frac{1}{m\omega_n}\frac{\lambda}{2(\lambda^2+\mu^2)}$.

We are interested in whether $h(0)$ can be zero or not. A piece of the function $h(0)$ versus α_{L} and α_{H} for $\eta = 0.1$ is shown in Fig. 6. There exist indeed combinations of α_{L} and α_{H} which lead to $h(0) = 0$. The solid thick line in the figure stands for $h(0) = 0$. We can see that for $0.7 < \alpha_{\mathrm{L}} > 1$, the α_{H} is limited and quite close to 1. This means that the pass band is rather narrow.

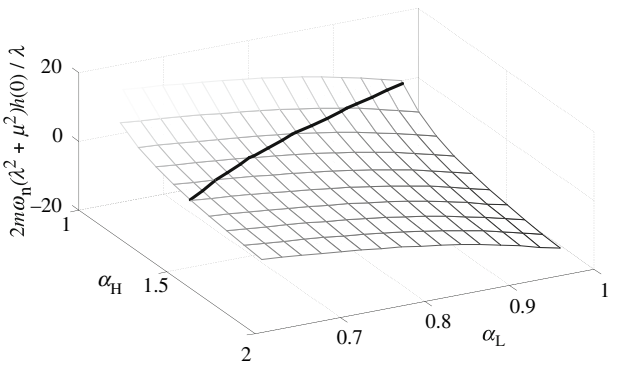

Fig. 6. Mesh plot of $h(0)$ versus α_{L} and α_{H} . $\eta = 0.1$. The *solid thick line* stands for $h(0) = 0$

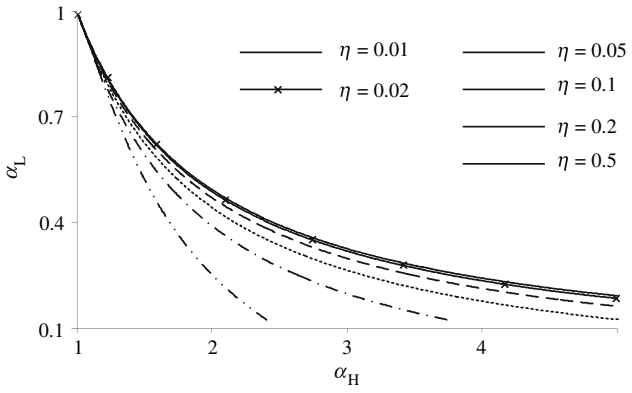

Fig. 7. Lower bounds varying vs. upper bounds for $h(0) = 0$

Figure 7 illustrates how the α_L and α_H combining on the 2-D plane leads to $h(0) = 0$. Six typical cases of $\eta = 0.5, 0.2, 0.1, 0.05, 0.02$ and 0.01 are plotted in this figure. Generally, the six lines show that as α_H increases, α_L decreases, except for a very small α_H. But it should always be kept in mind that the IRP is a nonzero function, even if $h(0)$ is zero.

6 Conclusion

The rate-independent damping model, one of the hysteretic models, is non-causal. However, its mathematical conciseness is so elegant that one wishes to alleviate the problem, rather than discarding the model completely. The modified model – the LBLHV – is studied systematically by means of the residue theorem in this report. It is shown that the IRP is not zero for a negative time instant, thus the model is non-causal. Ironically the effect of its non-causality can be even more serious than that of the ideal case. Similar to the ideal hysteretic, the asymptotic attenuating rate of the IRP is $O(1/t)$ as time approaches negative infinity. However, in contrast to the monotonic trend of the ideal hysteretic model, the IRP is composed of two oscillating components. The causal part is dominated by the component pertaining to the natural frequency. The band-limit parameters influence the first causal peak significantly. Unlike the ideal case, the response at $t = 0$ can achieve zero by appropriately choosing the lower and upper bounds of the pass band. The effect of the IRP is not monotonic, thus even if the response at $t = 0$ is zero, the IRP may be dramatic.

Acknowledgments

We thank the reviewer for the valuable comments and Mr. E. Koht for his kind help with English. We are also indebted to Prof. Maia for providing the relevant references and valuable comments.

References

[1] Kelly, J.M.: The role of damping in seismic isolation. Earthq. Engng. Struct. Dyn. **28**, 3–20 (1999)
[2] Priestley, M.J.N., Grant, D.N.: Viscous damping in seismic design and analysis. J. Earthq. Engng. **9**(special issue 2), 229–255 (2005)
[3] Kim, S.M., Cho, Y.H.: Vibration and dynamic buckling of shear beam-columns on elastic foundation under moving harmonic loads. Int. J. Solids. Struct. **43**, 393–412 (2006)
[4] Crandall, S.H.: The role of damping in vibration theory. J. Sound Vib. **11**, 3–18 (1970)

[5] Maia, N.M.M., Silva, J.M.M., Ribeiro, A.M.R.: On a general model for damping. J. Sound Vib. **218**, 749–767 (1998)
[6] Adhikari, S.: Dynamics of nonviscously damped linear systems. J. Engng. Mech. ASCE **128**, 328–339 (2002)
[7] Pritz, T.: Frequency power law of material damping. Appl. Acoust. **65**, 1027–1036 (2004)
[8] Park, D., Hashash, Y.M.A.: Soil damping formulation in nonlinear time domain site response analysis. J. Earthq. Engng. **8**, 249–274 (2004)
[9] Sherif, H.A., Abu Omar, T.M.: Mechanism of energy dissipation in mechanical system with dry friction. Tribol. Int. **37**, 235–244 (2004)
[10] Inaudi, J.A., Kelly, J.M.: Linear hysteretic damping and the Hilbert transform. J. Engng. Mech. ASCE **121**, 626–632 (1995)
[11] Muravskii, G.B.: On frequency independent damping. J. Sound Vib. **274**, 653–668 (2004)
[12] Crandall, S.H.: Dynamic response of systems with structural damping. In: Lees, S. (ed.) Air, Space and Instruments, Draper Anniversary, pp. 183–193. McGraw-Hill, New York (1963)
[13] Gaul, L., Bohlen, S., Kempfle, S.: Transient and forced oscillations of systems with constant hysteretic damping. Mech. Res. Commun. **12**, 187–201 (1985)
[14] Milne, H.K.: The impulse response function of a single degree of freedom system with hysteretic damping. J. Sound Vib. **100**, 590–593 (1985)
[15] Jones, D.I.G.: Impulse response function of a damped single degree of freedom system. J. Sound Vib. **106**, 353–356 (1986)
[16] Spencer, B.F.J., Bergman, L.A.: Stochastic response of systems with linear hysteretic damping. In: Proc. 11th Conf. on Engineering Mechanics Fort Lauderdale, FL, pp. 677–680 (1996)
[17] Chen, J.T., You, D.W.: Integral–differential equation approach for the free vibration of a SDOF system with hysteretic damping. Adv. Engng. Softw. **30**, 43–48 (1999)
[18] Tsai, H., Lee, T.: Dynamic analysis of linear and bilinear oscillators with rate-independent damping. Comput. Struct. **80**, 155–164 (2002)
[19] Makris, N.: Causal hysteretic element. J. Engng. Mech. ASCE **123**, 1209–1214 (1997)
[20] Muravskii, G.B.: Linear models with nearly frequency independent complex stiffness leading to causal behavior in time domain. Earthq. Engng. Struct. Dyn. **33**, 13–33 (2006)
[21] Ribeiro, A.M.R., Maia, N., Silva, J.M.: Free and forced vibrations with viscous and hysteretic damping: a different perspective. In: Proc. MZD-5th Int. Conf. Mechanics & Materials in Design, July 2006, Oporto, Portugal (2006)
[22] Nakamura, N.: Practical causal hysteretic damping. Earthq. Engng. Struct. Dyn. **36**, 597–617 (2007)
[23] Wolf, J.P., Darbre, G.R.: Time-domain boundary element method in viscoelasticity with application to a spherical cavity. Soil Dyn. Earthq. Engng. **5**, 138–148 (1986)
[24] Kang, Y.S., Kim, K.J.: Friction identification in a sight stabilisation system at low velocities. Mech. Syst. Signal Process. **11**, 491–505 (1997)
[25] Filiatrault, A., Isoda, H., Folz, B.: Hysteretic damping of wood framed buildings. Engng. Struct. **25**, 461–471 (2003)
[26] Verruijt, A., Cordova, C.C.: Moving loads on an elastic half-plane with hysteretic damping. J. Appl. Mech. Trans. ASME **68**, 915–922 (2001)
[27] Henwood, D.J.: Approximating the hysteretic damping matrix by a viscous matrix for modelling in the time domain. J. Sound Vib. **254**, 575–593 (2002)
[28] Muscolino, G., Palmeri, A., Ricciardelli, F.: Time-domain response of linear hysteretic systems to deterministic and random excitations. Earthq. Engng. Struct. Dyn. **34**, 1129–1147 (2005)
[29] Bishop, R.E.D., Price, W.G.: A note on hystereric damping of transient motions. Random vibration-status and recent developments, pp. 39–45. Elsevier, Amsterdam (1986)
[30] Crandall, S.H.: Hysteretic damping model in vibration theory. Proceedings of the Institution of Mechanical Engineers, Part C. Mech. Engng. Sci. **205**, 23–28 (1991)
[31] Crandall, S.H.: Ideal hysteretic damping is noncausal. Zeitschrift fuer Angewandte Mathematik und Mechanik ZAMM (Appl. Math. Mech.) **77**, 711 (1997)
[32] William, W.H., Teukolsky, S.A., Vetterling, W.T.: Numerical Recipes in C – The Art of Scientific Computing, 2nd edn. pp. 222–226. Cambridge University Press, UK (1998)
[33] Chen, K.F., Zhang, S.W.: On the impulse response precursor of an SDOF ideal linear hysteretic damper. J. Sound Vib. DOI: 10.1016/j.jsv.2007.07.091